Int. J. Electrochem. Sci., 13 **(2018)** 5253 – 5267, doi: 10.20964/2018.06.75

International Journal of
ELECTROCHEMICAL
SCIENCE
www.electrochemsci.org

Promotion Effects of CNTs-MnO_2 Nanowires-composite on Direct Electron Transfer of Hemoglobin for Amperometric H_2O_2 Determination

Chuan-yin Liu[1,2,*], *En-yong Shi*[1], *Ji-ping Yao*[1], *Rong Peng*[1]

[1] School of Chemical Engineering and Food Science, Hubei University of Arts and Sciences, Xiangyang 441053, P.R. China
[2] Hubei Key Laboratory of Low Dimensional Optoelectronic Materials and Devices, Xiangyang 441053, P.R. China
[*]E-mail: liucyin2002@sina.com

Received: 5 February 2018 / *Accepted:* 31 March 2018 / *Published:* 10 May 2018

MnO_2 nanomaterials with controlled morphologies were synthesized by different methods and characterized by SEM, XRD. The promotion ability of as-prepared MnO_2 nanomaterials towards the direct electron transfer (DET) of hemoglobin has been studied. It is found that promotion effect of carbon nanotubes (CNTs) and MnO_2 nanowires nanocomposite can be observed for the DET of hemoglobin. In the optimum conditions, the symmetrical redox peak can be observed with peak separation of 58 mV and formal potential of -0.339 V, respecting the direct electron transfer of hemoglobin on this composite film. The rate constant has also been estimated to be 1.10 s^{-1}. The proposed biosensor has favorable reproducibility, stability and sensitivity, and has been used to amperometric determination of hydrogen peroxide with detection limit of 2.4×10^{-8} mol/L, and the Michealis-Menten constant can also be estimated to be 0.32 mmol/L.

Keywords: CNTs-MnO_2 nanowires nanocomposite; Hemoglobin; Direct electron transfer; Hydrogen peroxide

1. INTRODUCTION

Since Eddowes [1] and Yeh [2] reported the DET of cytochrome c by electrochemical methods in 1977, the DET investigation between redox proteins and electrode has received considerable attentions in recent years. The mechanism of DET of redox proteins on electrode surface and the corresponding electrocatalytic reactions can provide an approach and methodology to understand the metabolic processes in biological systems [3]. In addition, redox-active proteins can be potentially

applied to fabricate electrochemical biosensors, catalytic bioreactors and bioelectroanalytical devices [4]. However, the electroactive center is deeply buried into the protein structure, and also the proteins may be easily to denature, it is difficult for redox proteins to achieve DET on the bare solid electrodes [5]. In order to accomplish the DET and to fabricate the third-generation biosensors, various methodologies have been used to enhance the DET by modification of bare electrode with nanomaterials and biocompatible films, such as g-C3N4 decorated Co2Al layered double hydroxide nanosheets [6] , graphene and nitrogen incorporated reduced graphene [7-8], quantum dots [9], metal nanoparticles [10], metal oxide nanoparticles [11] and inorganic-organic nanocomposite [12], inorganic-organic sol-gel [13], ionic liquid-graphene-NiO hollowsphere composite [14] and so on. The biocompatible films on the electrode surface can offer a kind of suitable microenvironment for the proteins to maintain its natural structure and the modified nanomaterials can accelerate the DET between proteins and the underlying electrode [15].

Recently, owing to their ion-changing, molecular adsorption, catalytic, electrochemical and magnetic properties, considerable research has been focused on the use of transition metal oxide-based catalysts to replace noble metal catalysts. In those transition metal oxides, manganese oxides are very attractive and have been extensively utilized as mediating or catalytic substance for electrochemical applications [16-20] due to their low cost, high activity, and nontoxicity. Because of their distinctive properties, α-, β-, γ-, and δ-type MnO_2 with different morphologies has been used as catalysts and electrode materials in Li/MnO_2 batteries. Moreover, it is found that MnO_2 with well-controlled dimensionality, size, and crystal structure may bring some novel and unexpected properties, as isotropic or anisotropic behavior, region-dependent surface reactivity and so on. Therefore, it is urgently important to develop morphologically controllable synthesis of MnO_2 nanoparticles and to explore the potential application of MnO_2. However, in the practical research, it is still a challenge to synthesize MnO_2 with peculiar morphology and phase and to control the oriented growth of MnO_2 nanostructures.

Although many studies have been reported to fabricate nonenzymatic amperometric hydrogen peroxide sensor using MnO_2 nanomaterials[15], which indicate that the electrocatalytic properties depend mainly on its crystalline structures and morphology [21]. However, to our best knowledge, few studies focused on the direct electrochemistry of redox proteins based on controlled synthesis of nano-MnO_2 with different crystalline structures and morphology, and synergistic promotion effect of CNTs and MnO_2 nanocomposite. Zhu [22] used urchinlike MnO_2 nanoparticles and chitosan and hemoglobin to modify carbon ionic liquid electrode, the direct electrochemistry of hemoglobin was achieved with redox peak separation of 140 mV and formal potential -0.180 V. The electron transfer coefficient (a) and the apparent heterogeneous electron transfer rate constant (k_s) were calculated as 0.325 and 0.406 s^{-1}. Zhang [23] used β-MnO_2 nanowires and glucose oxidase (GOx) to modify GCE, the modified GCE showed excellent electrocatalytic activity towards H_2O_2. The biosensor enables amperometric detection of glucose with a sensitivity of 38.2 μA mM^{-1} cm^{-2}, and a response time of <5 s. Xiao [11] used MnO_2 nanosheets to immobilize HRP, favorable redox peaks were achieved with formal potential of -0.350 V and heterogeneous electron transfer constant of 6.86 s^{-1}. The biosensor showed favorable electrocatalysis towards H_2O_2 with a detection limit of 0.21 μmol/L. Kim [24] used hierarchical MnO_2 with mesoporous structure and good biocompatibility for the immobilization of GOx. The favorable

reversible redox peaks with peak separation of 21 mV and formal potential of -0.453 V, heterogeneous electron transfer constant of 11.6 s^{-1} were achieved. The bioconjugate of a GOx/MnO_2-modified electrode was successfully employed for the mediatorless biosensing of glucose with sensivity of 31.6 mA mM cm^{-2}. Amreen [25] utilized blood and MnO_2 modified electrode system to detect dissolved oxygen and hydrogen peroxide, the detection value is comparable to that of a commercial dissolved oxygen measurement kit.

In this paper, nano MnO_2 were synthesized by several methods to obtain different morphologies, the prepared nano-MnO_2 were used as modifier to enhance the DET of Hb at glassy carbon electrodes. It is found that MnO_2 nanowires can effectively enhance the DET of Hb. To further investigation of synergistic effects of CNTs and nano-MnO_2, the CNTs-MnO_2 nanowires were firstly modified onto the electrode to construct electroactive interface, then Hb was entrapped in TiO_2 sol to construct the biocompatible film. It is found that the composite film can effectively enhance the DET of Hb comparing with that of mono-modification of MnO_2 nanowires and CNTs film, the favorable DET can be achieved with peak separation of 58 mV with formal potential of -0.339 V and heterogeneous electron transfer constant of 1.10 s^{-1}. The proposed biosensor resulted in excellent sensitivity, favorable stability and reproducibility, wide linear range and low detection limit towards H_2O_2 and low Michealis-Menten constant.

2. EXPERIMENTAL

2.1 Chemicals and Instruments

Hemoglobin (Hb), dopamine (DA), chitosan (CS), uric acid (UA), ascorbic acid (AA), potassium permanganate, $(NH_4)_2S_2O_8$, manganese sulfate, tetra-n-butyl titanate (TBT), H_2O_2 (30%) and other chemicals were purchased from Shanghai chemical reagent Co. (Shanghai, China), all the reagents are of analytical grade and used as received. 0.1 mol/L Phosphate Buffer Solution (PBS) was prepared by NaH_2PO_4 and Na_2HPO_4, and the pH was adjusted by H_3PO_4 and NaOH to a necessary value. 10 mg/ml Hb was prepared by dissolving Hb in pH 7 PBS. Carbon nanotubes (CNTs) with 95% purity were obtained from Nanotechnical Institute of Huazhong Normal University (Wuhan, China), and it was pretreated according to the reference [26] procedure with some modifications. The electrochemical cell was bubbled with high purity of N_2 for 15 min before usage and kept under N_2 atmosphere during measurements to eliminate the influence of dissolved oxygen. Double-distilled water was used throughout.

All the electrochemical experiments were carried out on a CHI 660A electrochemical workstation (USA) with conventional three-electrode cell, bare and modified glassy carbon electrode (GCE) was used as working electrode, saturated Ag/AgCl electrode as reference and Pt wire electrode as the counter electrode. The morphologies and crystalline phase characterization of MnO_2 nanowires were performed at S-4800 scanning electronic microscopy (SEM, S-4800, Hitachi, Japan) and Rigaku D/max rA X-ray diffractometer (XRD, Japan) equipped with graphite monochromatized high-intensity Cu Kα radiation (λ=1.54178 Å), FTIR (Shimadzu, Japan), UV spectrometer (Shimadzu, Japan).

2.2 Preparation of MnO_2 with different morphologies

MnO_2 with different morphologies were prepared by chemical precipitation and hydrothermal methods according to reference [27-28] with some modifications. The prepared MnO_2 was characterized by SEM, XRD and FTIR.

2.3 Preparation of TiO_2 sol

5 mL TBT and 5 mL 0.5% CS were added into a container with vigorous mixing and ultrasonic mixed for 60 min to a homogeneous solution and was subsequently stored at room temperature for 3 h. The pH value of sol was adjusted to 5.0 before usage. Then 100 μL Hb and 100 μL TiO_2 were mixed in a PVC tube under ultrasonic to form TiO_2-Hb sol.

2.4 Preparation of Hb modified electrode

The GCE (ϕ=2 mm) was polished with Al_2O_3 slurry to mirror-finish, and then it was sonicated with acetone and double-distilled water for 5 min, respectively. 10 μL of CNTs-MnO_2 nanowires suspension was coated on the GCE with a microsyringe, and the electrode was dried under an infrared lamp, then 10 μL Hb-TiO_2 sol was coated onto the surface of CNTs-MnO_2 modified GCE, dry-stored for 10 h at 4 ^oC (CNTs-MnO_2-TiO_2-Hb/GCE). For comparison, the Hb-TiO_2/GCE and CNTs-TiO_2-Hb/GCE were prepared using the same procedure only omitting the step of adding CNTs and nanowires MnO_2, respectively. All resulting electrodes were washed with water and dry stored at 4 ^oC refrigeratory when not in use.

2.5 Electrochemical characterization and measurements

The electrochemical characterization and measurements were performed with modified GCE as working electrode. Cyclic voltammetry was carried out in the potential range from -0.8 V to 0. 5 V. Alternative current impedance was performed in 0.1 mol/L KCl solution containing 1 mmol/L $Fe(CN)_6^{3-}$. The frequency range was from 0.01 Hz to 10^5 Hz, and the applied potential was set at the formal potential of $Fe(CN)_6^{3-/4-}$. The charge-transfer resistance can be fitted by the Zview® software.

3. RESULTS AND DISCUSSION

3.1 SEM, XRD and FTIR characterization of nano MnO_2 and UV characterization of mixed Hb solutions

The morphologies of MnO_2 prepared under different synthetic methods can be found in Figure 1. From Fig.1A and 1B, the particles with diameters >100 nm were synthesized by $MnSO_4$ and $(NH_4)_2S_2O_8$ under different reaction temperature and drying time.

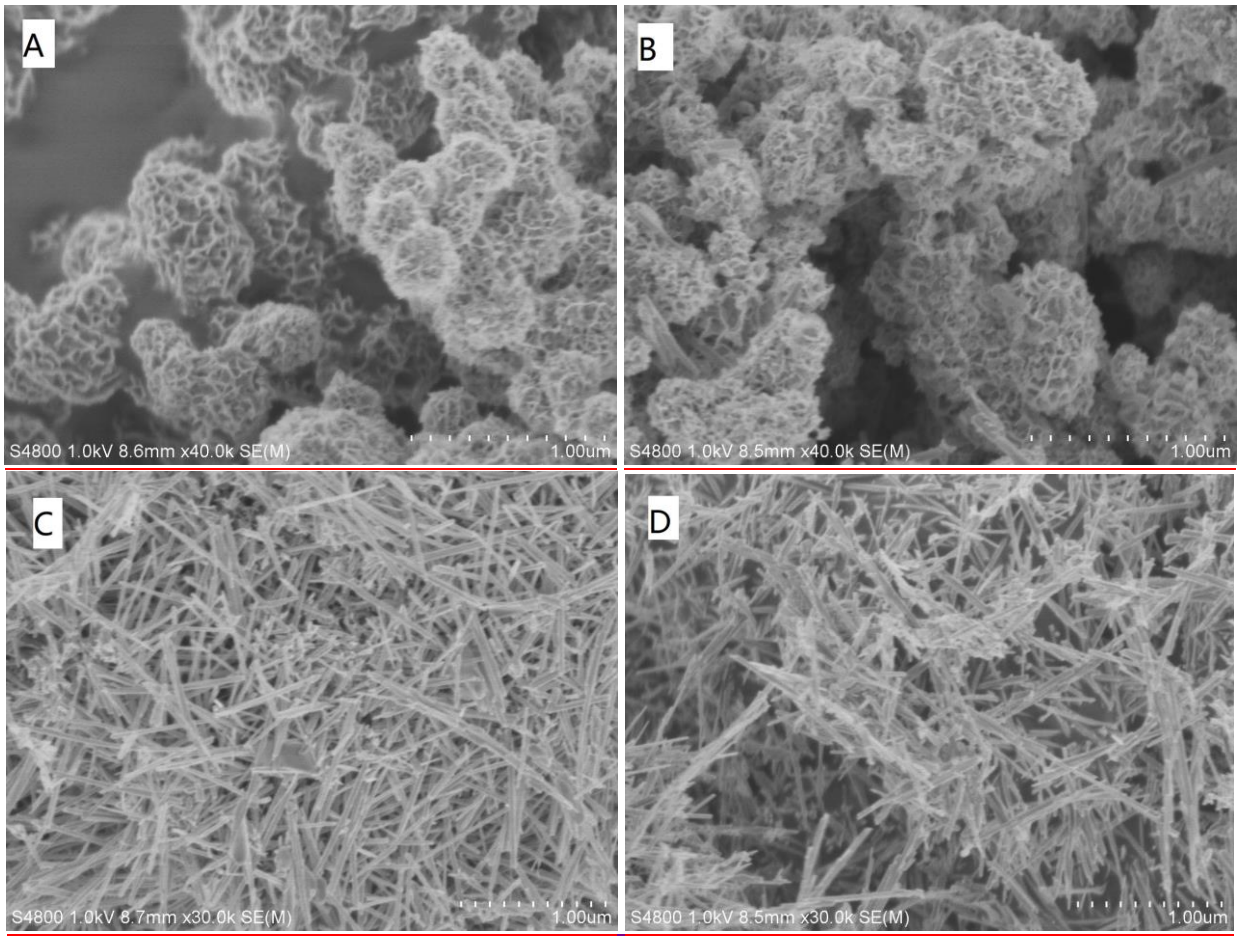

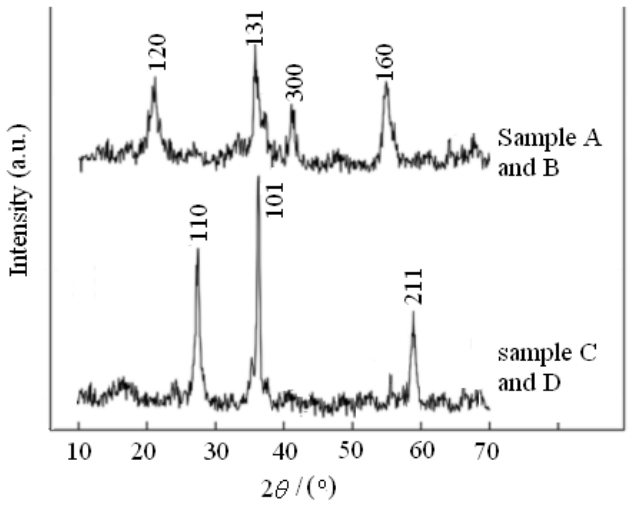

Figure 1. SEM and XRD of prepared MnO_2 (A and B stand for MnO2 synthesized by $MnSO_4$ and $(NH_4)_2S_2O_8$ under 140℃ for 17 h and 170℃ for 5.5 h, respectively; C and D stand for MnO2 synthesized by $MnSO_4$ and $KMnO_4$ under 80℃ for drying time 4 h and 8 h, respectively)

From Fig.1C and 1D, the nanowires with length of 1 μm and diameter of 30-40 nm were synthesized by $MnSO_4$ and $KMnO_4$ under 80℃ for different drying time. It can be seen that the MnO_2 nanowires are almost equal in length and tightly arranged (Fig.1C), however, there are some multidimensional branches in sample D (Fig.1D). It is obvious that the surface area of MnO_2 particles

(Fig.1A and 1B) is much smaller than those of nanowires, also the electrocatalytical properties towards DET of Hb are evaluated by cyclic voltammetry and amperometry. It is found that the surface area and electrocatalytical ability of particles is much smaller than that of nanowires. As for the comparative modification with 1C and 1D, the DET of 1C is much stronger than that of 1D. So in the latter experiments, nanowires of MnO_2 (1C) was used throughout to fabricate the proposed biosensors.

The XRD characterization of as-prepared MnO_2 nanomaterials can also be found in Figure 1. Sample A and B, the diffraction peaks at 2θ value of 21.710, 36.300, 41.750, 54.870, 64.105° are accordance to the standard figure of γ-MnO_2. However, the diffraction peaks of sample C and D at 27.455, 36.125, 49.240° are accordance with the standard figure of β-MnO_2.

The FTIR spectra of CNTs and CNTs-MnO_2 nanocomposite are shown in figure 2. It is found that activated CNTs have more absorption peaks than that of in-activated CNTs, the wide peak at 3425 cm^{-1} is corresponding to stretching vibration of –OH group, which may be attributed to the acid-activation of CNTs. While the peaks at 1705 cm^{-1} and 1400 cm^{-1} are attributed to the stretching vibration of C=O and bending vibration of -OH on the -COOH group, respectively. All the results indicated that CNTs have been activated and introduced -COOH and -C-OH onto CNTs. As for CNTs-MnO_2 nanocomposite, peaks at 3430 cm^{-1} and 1630 cm^{-1} are attributed to stretching and bending vibration of -OH group respectively, while the strong absorption peak at 582 cm^{-1} is attributed to the stretching vibration of Mn-O bond.

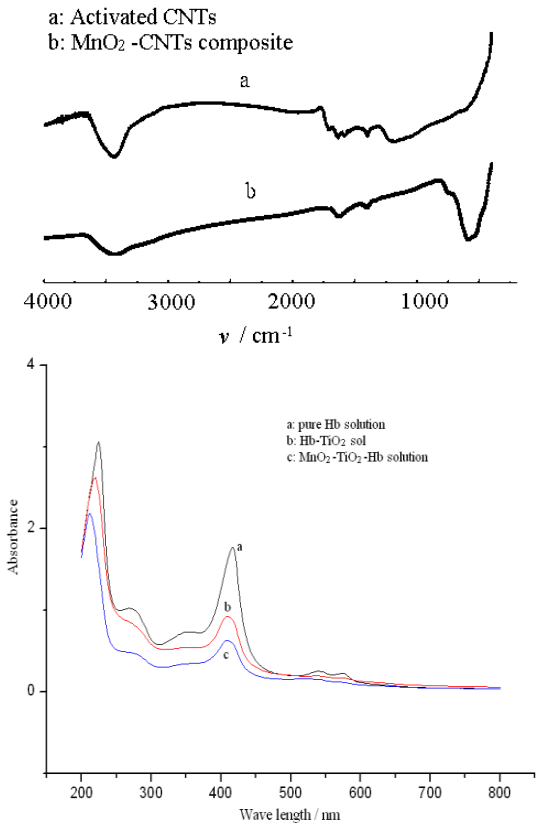

Figure 2. FTIR spectra of CNTs, CNTs-nanowires MnO_2 and UV spectra of Hb, TiO_2-Hb and MnO_2-TiO_2-Hb

The denaturing of redox proteins will exert adverse effect on DET investigation, the influence of MnO_2 nanowires on the bioactivity of Hb is also studied by UV spectroscopy. Form the UV spectra of pure Hb, TiO_2-Hb and MnO_2-TiO_2-Hb, it is found that the soret absorption peak (λ_{max}) is almost unaltered, manifesting that the natural structure of Hb has been effectively maintained with modification of MnO_2 nanowires.

3.2 Electrochemical characterization of modified electrodes

Cyclic voltammetry and electrochemical impedance spectroscopy are the effective methods to characterize the modification process of electrode. The cyclic voltammograms of bare GCE, CNTs-MnO_2/GCE and CNTs-MnO_2-TiO_2-Hb/GCE in 0.1 mol/L KCl containing 1 mmol/L $Fe(CN)_6^{3-}$ can be observed in Figure 3A. The reversible redox couples at bare GCE (ΔE_p=70 mV) and increased peak currents (ΔE_p=78 mV) with large capacitance current at CNTs-MnO_2/GCE appeared. The experimental results show the CNTs-MnO_2 wires nanocomposite can effectively enhance the practical area of modified GCE, the similar redox peak separation indicates the nanocomposite can promote the electron transfer across the electrode surface. However, the further modification of Hb in TiO_2 sol-gel on the CNTs-MnO_2, the peak currents of redox probe decreased dramatively with ΔE_p of 87 mV was observed, this variation may be attributed to the further modification of Hb-TiO_2 onto the CNTs-MnO_2/GCE, and Hb-TiO_2 film blocks the mass transfer of electroactive probe and contacting of probe with electrode surface.

For the Nyquist plots of the above three electrodes, based on the Zview simulation, charge transfer resistance (R_{ct}) bare GCE and CNTs-MnO_2/GCE was 128 and 184 Ω, respectively, indicating a diffusion controlled process was achieved and CNTs-MnO_2 did not hinder the probe from arriving at the electrode surface. However, a large semi-cycle in high frequency range with a fitting R_{ct} of 435 Ω was observed for CNTs-MnO_2-TiO_2-Hb/GCE, confirming the further modification of electrode with TiO_2-Hb and blocking effect of TiO_2-Hb film. It is clear that the electrochemical behavior of probe was controlled by charge transfer in high frequency. All the Nyquist plots are accordance to the cyclic voltammetric results.

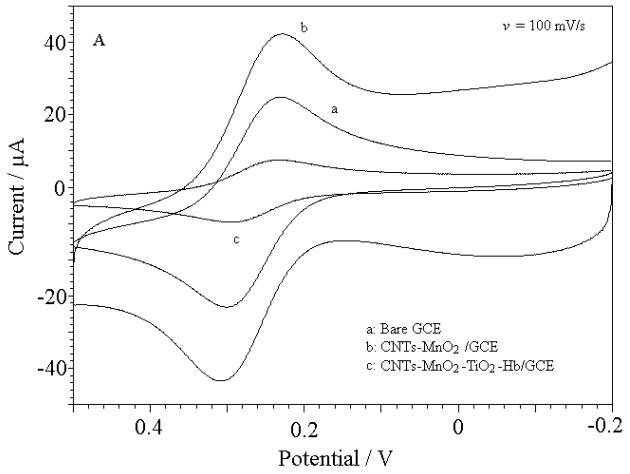

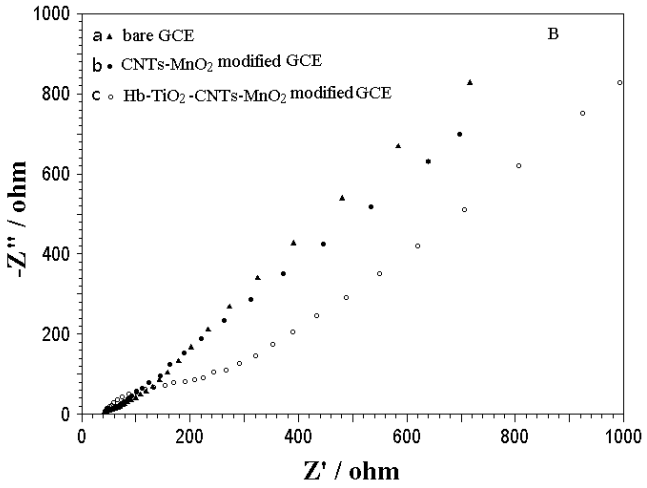

Figure 3. Cyclic voltammograms and Nyquist plots of bare GCE, CNTs-MnO_2/GCE and CNTs-MnO_2-TiO_2-Hb/GCE.

3.3 Direct electron transfer of Hb

Figure 4 shows the cyclic voltammograms of TiO_2-Hb/GCE, CNTs-TiO_2-Hb/GCE and CNTs-MnO_2-TiO_2-Hb/GCE in pH 7 PBS. From curve a, no redox peaks appear in TiO_2 sol-gel films, indicating that the electroactive center of Hb cannot achieve DET at biocompatible TiO_2 film, so it is necessary to construct electrocatalytic or electroactive layer to promote the DET of Hb. The modification of CNTs onto GCE surface, the Hb-TiO_2 sol-gel is further modified, a pairs of wide redox peaks can be observed at about 0 V to -0.2 V, this pair peaks can be attributed to the redox of carboxylic groups in carboxylic CNTs, and implies that the surface of the CNTs had been activated [29]. Another pairs of wide and weak peaks can also be seen in -0.2 V to -0.45 V range, this weak peak indicate that electroactive center of Hb can accomplish weak DET between Hb Fe center and the surface of CNTs modified electrode. However, as can be seen from curve c, except for a pair of wide peaks (about 0 to -0.2 V, this peaks attributed to redox of carboxylic groups of CNTs), another pair of symmetrical redox peaks appeared with E_{pa}=-0.310 V and E_{pc}=-0.368 V. This pair of peaks' current is almost equal with ΔE_p of 58 mV and formal potential of $E^{o/}$=-0.339 V ($E^{o'} = (E_{pa} + E_{pc})/2$) for CNTs-$MnO_2$-$TiO_2$-Hb/GCE. Obviously, this pair of redox peaks arises from the redox of the heme Fe centre of Hb embedded in CNTs-MnO_2-TiO_2 film. The formal potential is very close to the value reported by other references. Sun CQ's group immobilized Mb and colloidal gold nanoparticles on a GCE by a Nafion film, and a pair of reversible redox peaks appeared with the formal potential of -0.373 V [30]. Wang's group fabricated Mb/MWCNTs/CS film and the direct electrochemistry of Mb with a formal potential of -0.323 V was achieved [31]. Lavany [32] fabricated a hydrogen peroxide biosensor based on HRP immobilized on Ni doped SnO_2 nanoparticles, the direct electrochemistry of HRP with formal potential of -0.395±0.002 V was obtained. Pineda's group reported the gold nanoparticles (AuNP) capped with three different molecular layers (citrate anions, 6-mercaptopurine and omega-mercaptoundecanoic acid) and the protein hemoglobin, a pair of quasi-reversible redox peaks appeared with formal potential of -0.37 V. They also found that the first Au nanoparticles layer of Hb

surroundings was vital important to electroactive Hb [33]. Different formal potential appeared in different reports may be attributed to the distance between catalytic layers and heme Fe centre and the microcircustance for the exposure level of heme Fe centre.

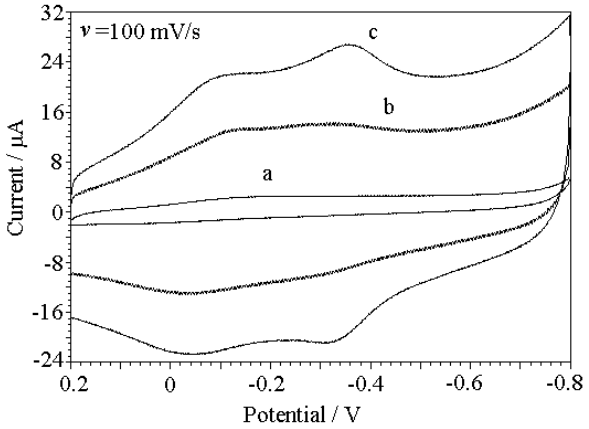

Figure 4. Cyclic voltammograms of TiO_2-Hb/GCE (a), CNTs-TiO_2-Hb/GCE (b) and CNTs-MnO_2-TiO_2-Hb/GCE (c).

3.4 Estimation of electron transfer process

Figure 5 is the cyclic voltammograms of CNTs-MnO_2-TiO_2-Hb/GCE under different scan rates and its further data-processing. From Fig. 5A, it can be found that the peak currents increased with square root of scan rate in 10-300 mV/s, and the peak currents were linear to square root of scan rates with a regression equation of I_{pa}=6.70-45.2$v^{1/2}$, r=0.9986; I_{pc}=-3.19+29.8$v^{1/2}$, r=0.9991 (Figure 5B). This result indicated that the electrochemical behavior of Hb immobilized on CNTs-MnO_2-TiO_2 film was a diffusion-controlled process [34]. It is also found that peak potentials varied with the scan rate in the range of 80-300 mV/s, while the formal potential kept almost unchanged. The regression equations were E_{pa}=-0.227+0.07468lg$v$, r=0.9919; E_{pc}=-0.4287-0.06181lg$v$, r=0.9936 (Figure 5C). As $n\Delta E_p \leq 200$ mV, the heterogeneous electron transfer rate constant can be estimated by Laviron equation [35].

$$E_{pc} = E^{o/} - \frac{2.3RT}{\alpha nF}\log\frac{\alpha nFk_s}{RT}v \quad E_{pa} = E^{o/} + \frac{2.3RT}{(1-\alpha)nF}\log\frac{(1-\alpha)nFk_s}{RT}v$$

$$\log k_s = \alpha\log(1-\alpha) + (1-\alpha)\log\alpha - \log(RT/nFv) - \alpha(1-\alpha)nF\Delta E_p / 2.3RT$$

According to the regression equations of E_p *vs*. log$v$, then na=0.95 and n(1-a)=0.79 can be estimated, assuming a=0.5, v=0.1 V/s and ΔE_p=0.58 V, the heterogeneous electron transfer constant k_s can be calculated to be 1.10 s^{-1}.

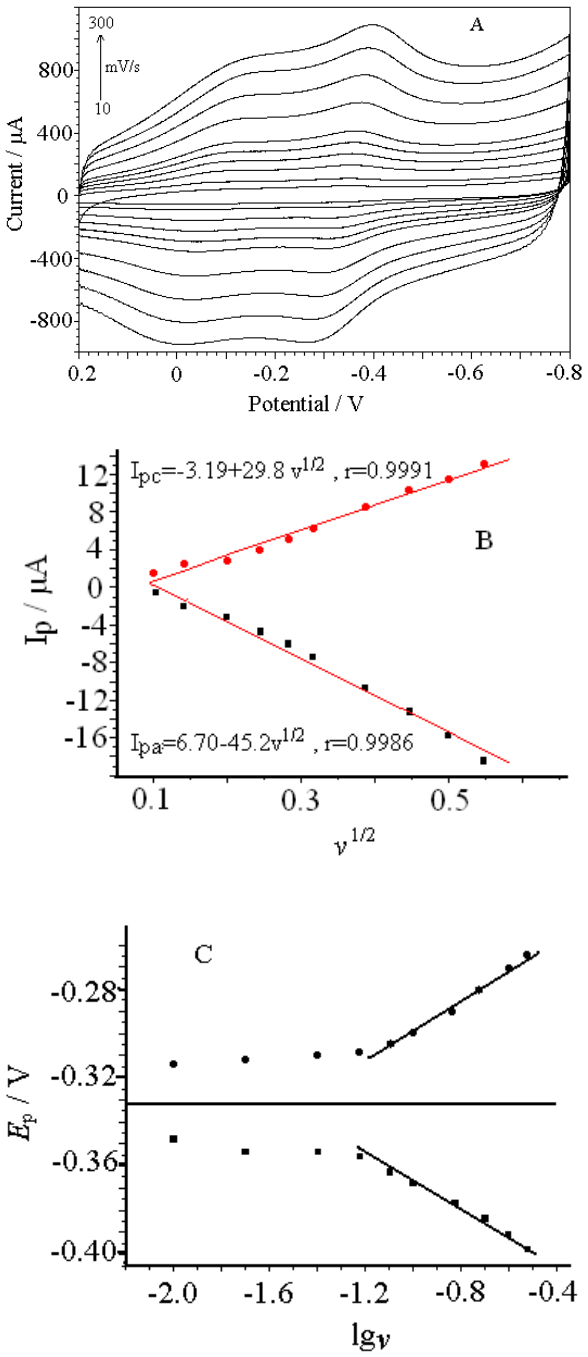

Figure 5. Cyclic voltammograms of CNTs-MnO_2-TiO_2-Hb/GCE at various scan rates (A), relationship between peak currents and square root of scan rates (B), relationship of peak potential *vs*. logarithm scan rate (C)

The calculated value is much higher than those previously reported on TiO_2 modified graphite electrode (0.62 s^{-1}) [36], Ag NPs doped CNTs modified gold electrode (0.41 s^{-1}) [37], CS-CNTs-Au NPs modified gold electrode(0.74 s^{-1}) [38], similar to that of $CoMoO_4$ nanorods modified carbon ionic liquid electrode (1.16 s^{-1}) [39] and lower than myogolobin immobilized on mesoporous carbon foam and salep hydrogel composite (2.25 s^{-1}) [40]. These results suggested that the electron transfer process

between the Hb molecules and CNTs-MnO_2-TiO_2 film was very fast. The result also manifests that with the composite can effectively decrease the distance among heme Fe centers and electrode surface, the presence of the CNTs-MnO_2 nanowires composite film is an excellent promoter to establish a fast electron transfer rate between the redox center of immobilized Hb and the electrode interface.

3.5 Optimization of the reaction conditions

The pH value of electrolyte will affect the three-dimension extending structure of protein, and will also affect the electrochemical response [38]. It is obvious that MnO_2 and CS cannot be stable under high acidity, and also the conformational change of Hb may happen in acid solution, so the pH value of electrolyte is chosen bigger than pH 4.0. To investigate pH effect on the electrochemical behavior of Hb in this composite film, in the pH range of 4.0-9.0, the peak currents of CNTs-MnO_2-TiO_2-Hb/GCE show linear relationship to pH value of electrolyte with regression equations of E_{pa}=0.04134-0.03902pH (R = 0.9962) and E_{pc}=-0.047-0.0436pH (R=0.9983), and the configuration changes are reversible. The phenomena indicated that the configuration changes were related to the H_2O and the protonation of amino acids around the heme group, which was defined as the Redox Bohr Effect [41]. The slope of formal potential *vs*. pH 41.3 mV/pH, was smaller than theoretical value of 57.6 mV/pH at 18 °C for a single-proton coupled, reversible one-electron transfer [42]. The phenomena might be attributed to the influence of the protonation states of trans ligands to the heme iron and amino acids around the heme, or the protonation of the water molecule coordinated to the central iron [43]. As CNTs-MnO_2-TiO_2-Hb/GCE has favorable and reversible electrochemical response at pH 7.0, so all the experiments were performed in pH 7.0 PBS unless specially stated.

Modification of GCE with different compositions and volumes of CNTs-MnO_2 have been tested for evaluation the electrochemical response of Hb by cyclic voltammetry. It is found that the concentration of MnO_2 in CNTs-CS solution is 3 mg/mL, the electrochemical response is the biggest. As the volume of MnO_2-CNTs increased from 1 μL to 10 μL, the response of electrode improved steadily. As the volumes of MnO_2-CNTs were larger than 10 μL, the response improved slowly with larger background current, which resulted in poor measure for H_2O_2. So the optimum loading of MnO_2-CNTs was chosen as 10 μL.

3.6 Electrocatalysis towards H_2O_2

The electrocatalytic activity towards H_2O_2 was also investigated by cyclic voltammetry and amperometric steady-state curves. It is found that the electrochemical reduction of H_2O_2 was started at -0.28 V and reached the biggest at -0.39 V under optimum conditions. Figure 6 is the amperometric steady state curves of CNTs-MnO_2-TiO_2-Hb/GCE towards H_2O_2. A regression equation of I (μA)=0.0622c(μmol/L)+0.072 with coefficient of 0.9984 has been achieved in the concentration range of 1.0×10^{-7} mol/L~2.0×10^{-4} mol/L, the detection limit can be calculated from 3σ of blank solution to be 2.4×10^{-8} mol/L.

When the H_2O_2 concentration was larger than 2.0×10^{-4}mol/L, a current plateau appeared, demonstrating a characteristic of Michaelis-Menten kinetic mechanism. The apparent Michaelis-Menten constant (K_m^{app}) can be calculated according to Linweaver-Burk equation [44-45],

$$\frac{1}{I_{ss}} = \frac{1}{I_{\max}} + \frac{K_m^{app}}{I_{\max} c}$$

Here, I_{max} is the maximum current under saturated substrate concentration, c is the concentration of H_2O_2. According to the regression equation $1/I_{ss} = 0.1465 + 47.10\, 1/c$, then the K_m^{app} can be estimated to be 0.32 mmol/L. The value is larger than that of 4.33 μmol/L for Hb immobilized on hollow MnS nanospheres [46], but similar to functionalized multi-walled carbon nanotube-poly-L-histine-ZnO nanocomposite film [47] and Mb/ZrO_2/MWCNT/GCE film [48]. The smaller value of K_m^{app} of present biosensor indicated that Hb immobilized in CNTs-MnO_2-TiO_2 film maintained favorable natural structure and affinity towards H_2O_2.

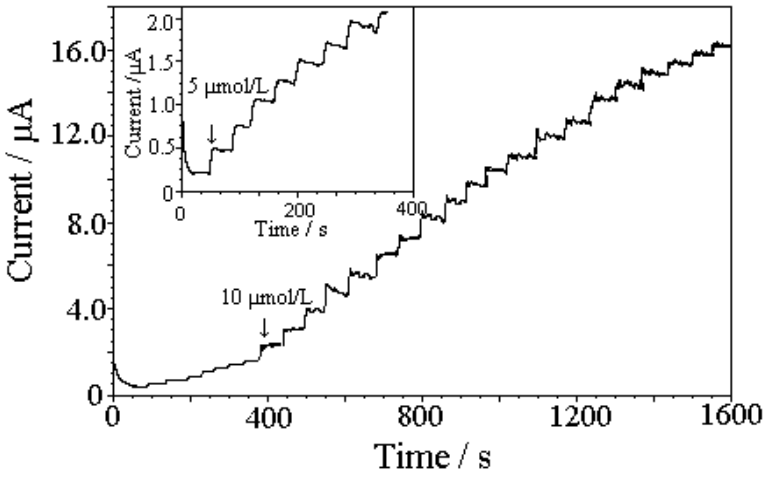

Figure 6. Amperometric curves of CNTs-MnO_2-TiO_2-Hb/GCE towards successively addition of hydrogen peroxide

3.7 Stability and reproducibility

The reproducibility of the composite film electrode was also investigated by cyclic voltammetry. When the electrode was successfully scanned for 11 cycles, the relative standard deviation (RSD) of peak currents was 3.2%. Under the optimum conditions, three electrodes were fabricated independently, showed an acceptable RSD of 4.7% for the current determination of 0.05 mmol/L H_2O_2. The long-term storage stability of the proposed biosensor was studied by monitoring the current of 0.05 mmol/L H_2O_2 every 3 days. The composite electrode retained its activity about 94% of its initial value after 30 days and about 83% after 50 days. All the reproducibility and stability could be attributed to CNTs-MnO_2-TiO_2 composite film providing desirable microenvironment and favorable biocatalytic ability for Hb immobilization.

3.8 Interference and real sample analysis

The electrochemical reduction of H_2O_2 is often interfered by other substances, such as DA, UA and AA. As for the proposed biosensor, amperometric steady-state curve has also been carried out at -390 mV for successive addition of DA, UA and AA to electrochemical cell, the catalytic current of H_2O_2 was used to evaluate the interference of those interfering substances. The amperometric responses of DA, UA and AA were very low as compared to equal amount of H_2O_2 at this applied potential. When adding 1.0 mmol/L AA, UA and DA to PBS containing 0.1 mmol/L H_2O_2, the current response for amperometric determination of H_2O_2 increased about 3.47%, 3.12% and 2.89%, respectively. The results also indicate that the biosensor has better selectivity.

As the proposed biosensor have better selectivity, reproducibility and stability, the real sample analysis for H_2O_2 by the present electrode has been carried out. The real sample (disinfector) was from Hubei Xiangyang Central Hospital, other simulated sample was prepared with urine and serum, real and simulated sample was added into pH 7 PBS to synthesize the working solution, and the determined value by this proposed method is very similar to that by fluorescence method, and the recoveries were in the range of 96.7%-102.8%.

Table 1. Recoveries of proposed biosensor for hydrogen peroxide determination

Sample	Conc. by fluorescence/μM	Conc. by this method/μM	Added μM	Detected μM	Recovery
Disinfector	3.23	3.31	1.00	0.978	97.8%
Urine+PBS+standard	2.51	2.52	1.00	1.015	101.5%
Serum+PBS+standard	2.48	2.51	1.00	1.028	102.8%

4. CONCLUSIONS

By controlling the synthetic methods and reaction conditions, different morphologies of MnO_2 nanomaterials have been prepared and were characterized by SEM, XRD. The prepared MnO_2 nanomaterials have been used to promote the direct electron transfer of hemoglobin, it is found that MnO_2 nanowires can effectively enhance the DET of hemoglobin, and further CNTs have been used to fabricate composite film to enhance DET. In the optimum conditions, the symmetrical redox peak can be observed with peak separation of 58 mV and formal potential of -0.339 V, respecting the direct electron transfer of hemoglobin on this composite film. The rate constant has also been estimated to be 1.10 s^{-1}. The proposed biosensor has favorable reproducibility, stability and sensitivity, and has been used to amperometric determination of hydrogen peroxide with detection limit of 2.4×10^{-8} mol/L, and the Michealis-Menten constant can also be estimated to be 0.32 mmol/L.

ACKNOWLEDGEMENT
The authors thanks the financial support of Open-fund of Hubei key laboratory of low dimensional materials and devices (13XKL02012).

References

1. M.J. Eddowes, H.A.O. Hill , *J. Chem. Soc. Chem. Commun*., 21(1977)771.
2. P. Yeh, T. Kuwana, *Chem. Lett*., 10(1977)1145.
3. F.A. Armstrong, G.S. Wilson, *Electrochim. Acta*, 45(2000)2623.
4. A.L. Ghindilis, P. Atanasov, E. Wilkins, *Electroanal.*, 9(1997)661.
5. G. Victor, L. Ovadia, *J. Am. Chem. Soc*., 115(1993)2533.
6. T.R. Zhan, Z.W. Tan, X.J. Wang, W.G. Hou, *Sens. Actuator B: Chem*., 255(2018)149.
7. A.T. Lawal, *Biosens. Bioelectron.*, 106(2018)149.
8. J. Lavanya, A. Subbiah, S. Neogi, N. Gomathi, *Sens. Actuators B: Chem.*, 255(2018)536.
9. X.L. Luo, A. Morrin, A.J. Killard, M.R. Smyth, *Electroanal.*, 18(2006)319.
10. D. Fapyane, E.E. Ferapontova, *Electrochem. Commun.*, 70(2016)39.
11. W.W. Mao, B. Cai, Z.Z. Ye, J.Y. Huang, *Sens. Acuators B: Chem.*, 261(2018)385.
12. G.Q. Zhang, T.W. Cao, H.S. Huang, P. Zhang, J. Appl. Electrochem., 46(2016)593.
13. R. Gupta, N.K. Chaudhury, *Biosens. Bioelectron.*, 22(2007)2387.
14. W.S. Zhao, X.Y. Li, Z.R. Wen, X.L. Niu, Q.F. Shen, Z.L. Sun, R.X. Dong, W. Sun, *Int. J. Electrochem. Sci.*, 12(2017)4025.
15. Y. Han, J.B. Zheng, S.Y. Dong, *Electrochim. Acta*, 90(2013)35.
16. B. Xu, M.-L. Ye, Y.-X. Yu, W.i-D. Zhang, *Anal. Chim. Acta*, 674(2010)20.
17. A.V. Eremenko, E.A. Dontsova, A.P. Nazarov, E.G. Evtushenko, S.V. Amitonov, S.V. Savilov, L.F. Martynova, V.V. Lunin, I.N. Kurochkin, *Electroanal.*, 24(2012)573.
18. Y.J. Yang, S.S. Hu, *Electrochim. Acta*, 55(2010)3471.
19. S.B. Hocevar, B. Ogorevc, K. Schachl, K. Kalcher, *Electroanal.*, 16(2004)1711.
20. W. Sun, X.Z. Wang, H.H. Zhu, X.H. Sun, F. Shi, G.N. Li, Z.F. Sun, *Sens. Actuators B: Chem.*,, 178(2013)443.
21. Y.H. Bai, H. Zhang, J.J. Xu, H.Y. Chen, *J. Phys. Chem. C*, 112(2008)18984.
22. Z.H. Zhu, L.N. Qu, Q.J. Niu, Y. Zeng, W. Sun, X.T. Huang, *Biosens. Bioelectron.*, 26(2011)2119.
23. L. Zhang, S.M. Yuan, L.M. Yang, Z. Fang, G.C. Zhao, *Microchim. Acta*, 180(2013)627.
24. P. Si, P. Chen, D.-H. Kim, *J. Mater. Chem. B*, 1(2013)2696.
25. K. Amreen, A.S. Kumar, *J. Electroanal. Chem*., 809(2018)36.
26. D. Chattopadhyay, I. Galeska, F. Papadimitrakopoulos, *Carbon*, 40(2002)985.
27. X. Wang, Y.D. Li, *Chem. Commun.*, 7(2002)764.
28. C.Z. Wu, Y. Xie, D. Wang, J. Yang, T.W. Li, *J. Phys. Chem. B*, 107(2003)13583.
29. L.Y. Jiang, R.X. Wang, X.M. Li, L.P. Jiang, G.H. Lu, *Electrochem. Commun.*, 7(2005)596.
30. W.W. Yang, Y.C. Li, Y. Bai, C.Q. Sun, *Sens. Actuators B: Chem.*, 115(2006)42.
31. L.S. Duan, Q. Xu, F. Xie, S.F. Wang, *Int. J Electrochem. Sci.*, 3(2008)118.
32. N. Lavanya, S.Radhakrishnan, C.Sekar, *Biosens. Bioelectron.*, 36(2012)41.
33. R. del Cano, L. Mateus, G. Sanchez-Obrero, J.M. Sevilla, R. Madueno, M. Blazquez, T. Pineda, *Talanta*, 176(2018)667.
34. A.J. Bard, L.R. Faulkner, John Wiley and Sons, New York, 2000
35. E. Laviron, *J. Electroanal. Chem.*, 101(1979)19.
36. W.J. Li, R. Yuan, Y.Q. Chai, L. Zhou, S.H. Chen, N. Li, *J. Biochem. Biophys. Methods*, 70(2008)830.
37. C.Y. Liu , J.M. Hu, *Biosen. Bioelectron.*, 24(2009)2149.
38. C.Y. Liu, J.M. Hu, *Electroanal.*, 20(2008)1067.
39. Z.Y. Zhao, L.L. Cao, A.H. Hu, W.L. Zhang, X.M. Ju, Y.Y. Zhang, W. Sun, *Bull. Korean Chem. Soc*., 34(2013)475.
40. M. Jahanbakhshi, *Microchim. Acta*, 185(2018)2654.
41. H.H. Liu, Z.Q. Tian, Z.X. Lu, Z.L. Zhang, M. Zhang, D.W. Pang, *Biosen. Bioelectron.*, 20(2004)294.

42. Y.X. Sun, S.F. Wang, *Bioelectrochem.*, 71(2007)172.
43. A.M. Bond, Marcel Dekker, New York, 1980.
44. C.I. Yamazaki, T. Araiso, Y. Hayashi, H. Yamada, R. Makino, *Adv. Biophys*., 11(1978)249.
45. R.A. Kamin, G.S. Willson, *Anal. Chem.*, 52(1980)1198.
46. S.Y. He, W.W. Qiu, L.H. Wang, F. Gao, W. Wang, Z.S. Hu, Q.X. Wang, *J. Mater. Sci.*, 51(2016)7156.
47. A.T.E. Vilian, S.M. Chen, C.H. Kwak, S.K. Hwang, Y.S. Huh, Y.K. Han, *Sens. Actuators B: Chem.*, 224(2016)607.
48. R.P. Liang, M.Q. Deng, S.G. Cui, H. Chen, J.D. Qiu, *Mater. Res. Bull*., 45(2010)1855.